ANS MC2015 - Joint International Conference on Mathematics and Computation (M&C), Supercomputing in Nuclear Applications (SNA) and the Monte Carlo (MC) Method · Nashville, Tennessee · April 19–23, 2015, on CD-ROM, American Nuclear Society, LaGrange Park, IL (2015)

A NON-NEGATIVE, NON-LINEAR, PETROV-GALERKIN METHOD FOR BILINEAR DISCONTINUOUS DIFFERENCING OF THE S_N EQUATIONS

Peter G. Maginot, Jean C. Ragusa*, and Jim E. Morel
Department of Nuclear Engineering
Texas A&M University
3133 TAMU, College Station, TX 77843
pmaginot@tamu.edu; jean.ragusa@tamu.edu; morel@tamu.edu

ABSTRACT

We have developed a new, non-negative, non-linear, Petrov-Galerkin discontinuous finite element method (NNPGDFEM), for use in conjunction with Galerkin bilinear discontinuous (BLD) finite element differencing of the 2-D Cartesian geometry S_N equations for quadrilaterals on an unstructured mesh. This work is an extension of the idea that drove our previous development of a NNPGDFEM for use with linear discontinuous (LD) differencing of the 2-D Cartesian geometry S_N equations for rectangular mesh cells. We present the theory and equations that describe the new method. Additionally, we numerically compare the accuracy of our proposed method to the accuracy of the BLD scheme (without lumping) and the subcell corner balance method (equivalent to a "fully" lumped bilinear discontinuous scheme) for a test problem in which the BLD solution contains negative angular flux solutions

Key Words: Radiation transport, DFEM, non-negative, bilinear, quadrilaterals

1 INTRODUCTION

Discontinuous finite element method (DFEM) spatial discretizations of the S_N neutron transport equation and S_N thermal radiative transfer equations can result in negative angular flux and negative angular intensity solutions. These negative solutions are non-physical, but inherent to the mathematics that define the radiation spatial differencing scheme. Several researchers have examined several different methods (matrix lumping [1], fix-ups [2], and strictly non-negative solution representations [3]) that inhibit or eliminate the negativities of the linear discontinuous (LD) finite element scheme on a variety of spatial mesh cell types (slab, rectangular, triangular, . . .), for the S_N neutron transport equation. However, Adams showed that LD does not maintain the neutronics thick diffusion limit on quadrilaterals [1]. We are interested in accurate methods for radiative transfer on quadrilaterals, therefore we seek methods that can maintain the radiative transfer equilibrium diffusion limit on quadrilaterals. If a radiative transfer spatial discretization is to maintain the equilibrium diffusion limit, its neutron transport analog must preserve the the thick diffusion limit. As a first step towards accurate methods for radiative transfer on quadrilaterals, we thus seek non-negative, bilinear discontinuous (BLD) finite element spatial discretizations of the neutron transport equation on quadrilaterals.

[*] Corresponding author

The Galerkin BLD spatial discretization for quadrilaterals, more commonly referred to as unlumped bilinear discontinuous (UBLD) yields negative angular flux solutions for spatial cells with glancing radiation incidence and/or large optical thickness [1]. To our knowledge, only matrix lumping has been considered in an attempt to inhibit negative angular flux solutions of BLD spatial discretizations. While more common forms of matrix lumping, such as mass matrix or combination mass and surface matrix lumping, inhibit negative angular flux solutions, they do not guarantee a strictly non-negative BLD angular flux solution [1]. Wareing, et. al, derived the fully lumped BLD (FLBLD) scheme [4], that uses additional manipulations of the UBLD equations to yield angular flux solutions that are strictly non-negative. Unfortunately, Adams demonstrated that FLBLD, which is equivalent to the subcell balance method on rectangles, is less accurate than the unlumped BLD (UBLD) scheme for spatial mesh cells of thin and intermediate thicknesses [5].

In [3], we developed a non-negative, non-linear Petrov-Galerkin DFEM for use in conjunction with LD spatial differencing of the S_N equations in slab and rectangular Cartesian geometry. In this paper, will extend the main idea of [3] to create a non-negative, non-linear Petrov-Galerkin DFEM to be used with UBLD spatial differencing on unstructured quadrilaterals. The remainder of this paper is divided as follows: a brief derivation common to all bilinear DFEM in Section 2, description and derivation of our new, bilinear consistent set-to-zero (BCSZ) Petrov-Galerkin scheme is given in Section 3, computational results demonstrating the strictly positive nature of BCSZ and its improved accuracy relative to UBLD and FLBLD are given in Section 4, and conclusions are given in Section 5.

2 MOMENT EQUATIONS

We begin by first considering the 2-D Cartesian discrete ordinates transport equation:

$$\vec{\Omega}_d \cdot \nabla\psi(x,y,\vec{\Omega}_d) + \sigma_t(x,y)\psi(x,y,\vec{\Omega}_d) = S_d(x,y)\,, \tag{1}$$

where $\vec{\Omega}_d$ is the neutron direction, $\psi(x,y,\vec{\Omega}_d)$ is the angular flux $[n/(cm^s\ sec\ ster)]$, $\sigma_t(x,y)$ is the total interaction cross section $[cm^{-1}]$, and $S_d(x,y)$ is the total source (scattering + fixed sources) in direction $\vec{\Omega}_d$. Following the standard Galerkin procedure, we take the spatial moment of Eq. (1) with respect to basis function $B_i(x,y)$ by first multiplying by basis function $B_i(x,y)$ and then integrating over the spatial cell K. Assuming cell-wise constant σ_t, the $i-$ th spatial moment equation is:

$$\int_K B_i(x,y)\left[\vec{\Omega}_d \cdot \nabla\psi(x,y,\vec{\Omega}_d) + \sigma_t\psi(x,y,\vec{\Omega}_d)\right]\,dxdy = \int_R B_i(x,y)S(x,y)\,dxdy\,. \tag{2}$$

Using integration by parts Eq. (2) becomes:

$$(\vec{\Omega}_d \cdot \vec{n})\oint_R B_i(x,y)\psi(x,y,\vec{\Omega}_d)\,dS - \int_R \psi(x,y,\vec{\Omega}_d)\left[\vec{\Omega}\cdot(\nabla_{xy}B_i(x,y))\right]dxdy \\ + \sigma_t\int_R B_i(x,y)\psi(x,y,\vec{\Omega}_d)\,dxdy\,. \tag{3}$$

Defining a reference element mapping as in Fig. 1: a reference point (s,t), $s\in[-1,1]$ $t\in[-1,1]$,

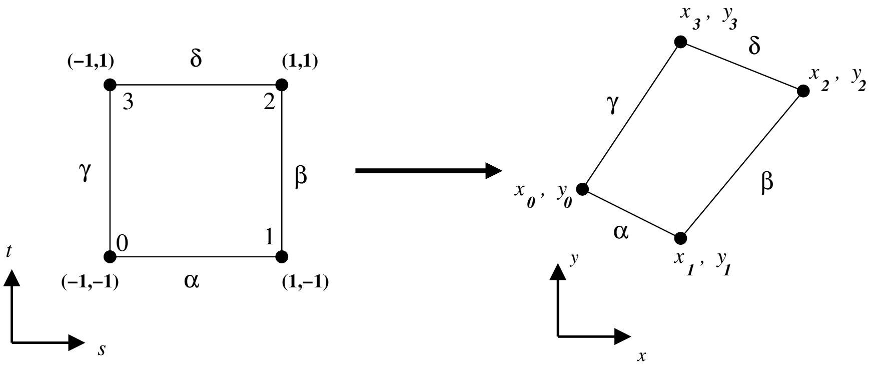

Figure 1. Reference element mapping.

is transformed to a physical point (x, y) such that:

$$x = x_0B_0(s,t) + x_1B_1(s,t) + x_2B_2(s,t) + x_3B_3(s,t) \tag{4}$$

$$y = y_0B_0(s,t) + y_1B_1(s,t) + y_2B_2(s,t) + y_3B_3(s,t)\,. \tag{5}$$

In this work, we use mapped, bilinear Lagrange interpolatory functions as our basis functions:

$$B_0(s,t) = \frac{1-s}{2}\frac{1-t}{2} \tag{6a}$$

$$B_1(s,t) = \frac{s+1}{2}\frac{1-t}{2} \tag{6b}$$

$$B_2(s,t) = \frac{s+1}{2}\frac{t+1}{2} \tag{6c}$$

$$B_3(s,t) = \frac{1-s}{2}\frac{t+1}{2}\,. \tag{6d}$$

As a result, following the Galerkin procedure creates four equations with many more unknowns than equations. To solve the exact moment equations, one must assume a solution representation, $\widetilde{\psi}(s, t, \vec{\Omega}_d)$, to approximate the true angular flux, $\psi(s, t, \vec{\Omega}_d)$.

The UBLD scheme assumes a solution trial space equal to the weight/basis space,

$$\widetilde{\psi}_{UBLD} = \sum_{i=0}^{3} \psi_{i,UBLD} B_i(s,t)\,. \tag{7}$$

Under this assumption, the spatial moments of the transport equation become a 4×4 linear system of equations. Interested readers are directed to [1] or one of the many other papers that have derived and used UBLD on rectangles and quadrilaterals for a more complete derivation.

The FLBLD [1,4] alternatively derived as the subcell balance method on quadrilaterals [5] begins with the UBLD equations then lumps (diagonalizes) the UBLD mass and surface matrices. The FLBLD equations are then further manipulated to result in a strictly non-negative solution representation that is second order convergent in space, and is found by solving a 4×4 linear system of equations. Again, the interested reader is directed to [1,4,5] for a more detailed derivation.

The BCSZ scheme is defined as being a bilinear function, $\widehat{\psi}_{BCSZ}$,

$$\widehat{\psi}_{BCSZ}(s,t) = \sum_{i=0}^{3} \psi_{i,BCSZ} B_i(s,t)\,, \tag{8}$$

everywhere $\widehat{\psi}_{BCSZ}$, is positive and zero otherwise:

$$\widetilde{\psi}_{BCSZ}(s,t) = \begin{cases} \widehat{\psi}_{BCSZ}(s,t) & \widehat{\psi}_{BCSZ}(s,t) > 0 \\ 0 & \text{otherwise} \end{cases} . \tag{9}$$

The initial iterate of $\widehat{\psi}_{BCSZ}$is $\widetilde{\psi}_{UBLD}$. If, and only if, $\widetilde{\psi}_{UBLD} \geq 0$ everywhere within a cell, $\widetilde{\psi}_{BCSZ} = \widetilde{\psi}_{UBLD}$. Using the definition of $\widetilde{\psi}_{BCSZ}$given in Eq. (9) turns the four spatial moments of the transport equation into four non-linear equations with four fundamental unknowns, $\psi_{i,BCSZ}$ that describe the bilinear function $\widehat{\psi}_{BCSZ}$.

3 BCSZ SCHEME

For brevity, we have omitted completely deriving the four spatial moment equations. Rather, we choose to focus on defining the important characteristics of the BCSZ scheme, namely how the BCSZ scheme defines the following moments equation quantities:

1. edge leakage, $\psi_{i,edge}$,
2. cell volume gradients, $\psi_{i\mu}$ and ψ_{η}, and
3. cell volume moments, $\psi_{i,M}$.

The $\psi_{i,edge}$ terms come from the moment equation integration by parts:

$$\begin{aligned}(\vec{\Omega}_d \cdot \vec{n}) \oint_R B_i(x,y)\psi(x,y,\vec{\Omega}_d)\,dS = (\vec{\Omega}_d \cdot \vec{n}_\alpha)\frac{|J_\alpha|}{2}\int_{-1}^{1} B_i(s,-1)\psi(s,-1)\,ds \\ + (\vec{\Omega}_d \cdot \vec{n}_\beta)\frac{|J_\beta|}{2}\int_{-1}^{1} B_i(1,t)\psi(1,t)\,dt + (\vec{\Omega}_d \cdot \vec{n}_\delta)\frac{|J_\delta|}{2}\int_{-1}^{1} B_i(s,1)\psi(s,1)\,ds \\ + (\vec{\Omega}_d \cdot \vec{n}_\gamma)\frac{|J_\gamma|}{2}\int_{-1}^{1} B_i(-1,t)\psi(-1,t)\,dt\,, \end{aligned} \tag{10a}$$

$$(\vec{\Omega}_d{\cdot}\vec{n}) \oint_R B_i(x,y)\psi(x,y,\vec{\Omega}_d)\,dS = (\vec{\Omega}_d{\cdot}\vec{n}_\alpha)\frac{|J_\alpha|}{2}\psi_{i,\alpha}+(\vec{\Omega}_d{\cdot}\vec{n}_\beta)\frac{|J_\beta|}{2}\psi_{i,\beta}+(\vec{\Omega}_d{\cdot}\vec{n}_\delta)\frac{|J_\delta|}{2}\psi_{i,\delta}+(\vec{\Omega}_d{\cdot}\vec{n}_\gamma)\psi_{i,\gamma}\,, \tag{10b}$$

where $|J|_z$ is the length of side z and $\vec{n}_z$ is the outward directed unit normal of side z. The cell volume gradients,$\psi_{i,\mu}$ and $\psi_{i,\eta}$ come from:

$$\int_R \psi(x,y,\vec{\Omega}_d)\left[\vec{\Omega}\cdot(\nabla_{xy}B_i(x,y))\right]dxdy = \vec{\Omega}_x \int_{-1}^{1}\int_{-1}^{1}\psi(s,t)\left(\frac{\partial y}{\partial t}\frac{\partial B_i}{\partial s}-\frac{\partial y}{\partial s}\frac{\partial B_i}{\partial t}\right)dsdt + \vec{\Omega}_y \int_{-1}^{1}\int_{-1}^{1}\psi(s,t)\left(\frac{\partial x}{\partial s}\frac{\partial B_i}{\partial t}-\frac{\partial x}{\partial t}\frac{\partial B_i}{\partial s}\right)dsdt \quad (11a)$$

$$\int_R \psi(x,y,\vec{\Omega}_d)\left[\vec{\Omega}\cdot(\nabla_{xy}B_i(x,y))\right]dxdy = \mu\psi_{i,\mu}+\eta\psi_{i,\eta}\,. \quad (11b)$$

The $\psi_{i,M}$ term comes from the reaction term:

$$\sigma_t\int_R B_i(x,y)\psi(x,y,\vec{\Omega}_d)\,dxdy = \sigma_t\int_{-1}^{1}\int_{-1}^{1}B_i(s,t)\psi\,|\mathbf{J}|\,dsdt = \sigma_t\psi_{i,M}\,. \quad (12)$$

In Eq. (11), all $\frac{\partial}{\partial s}$ terms are linear functions in t, all $\frac{\partial}{\partial t}$ terms are linear functions in s, $\mathbf{J}$ is the Jacobian matrix of the coordinate transformation:

$$\mathbf{J} = \begin{bmatrix} \frac{\partial x}{\partial s} & \frac{\partial y}{\partial s} \\ \frac{\partial x}{\partial t} & \frac{\partial y}{\partial t} \end{bmatrix}. \quad (13)$$

3.1 BCSZ Cell Integration

Given the definition of $\widetilde{\psi}_{BCSZ}$in Eq. (9), the integral contributions to $\psi_{i,\mu},\ \psi_{i,\eta},$ and $\psi_{i,M}$ are non-trivial only over a portion of the cell where $\widehat{\psi}_{BCSZ}(s,t) > 0$. There are seven possible geometric integration cases to be considered for all values of $\widehat{\psi}_{BCSZ}$. Six are shown in Fig. 2. The other case is when $\widehat{\psi}_{BCSZ} > 0$ everywhere in the cell, in which case the integration of $\psi_{i,\mu},\ \psi_{i,\eta},$ and $\psi_{i,M}$ is straight forward, and identical to that required by the defintion of the UBLD scheme. Though other cases are possible, all can be transformed into one of the cases in Fig. 2 via rotation. By definition, along each sold line in Fig. 2, $\widehat{\psi}_{BCSZ} = 0$. To evaluate $\psi_{i,\mu},\ \psi_{i,\eta},$ and $\psi_{i,M}$ over some region, R, in Fig. 2 where $\widehat{\psi}_{BCSZ} > 0$ and one edge is bounded by a curve, we use a variable limit of integration in t. To do this, we first transform $\widehat{\psi}_{BCSZ}$from an interpolatory polynomial to a moment based polynomial, $f(s,t)$:

$$f(s,t) = f_c + sf_s + tf_t + stf_{st}\,. \quad (14)$$

We find the coefficients of this formula using the interpolatory definition of the basis functions:

$$\begin{bmatrix} 1 & -1 & -1 & 1 \\ 1 & 1 & -1 & -1 \\ 1 & 1 & 1 & 1 \\ 1 & -1 & 1 & -1 \end{bmatrix}\begin{bmatrix} f_c \\ f_s \\ f_t \\ f_{st} \end{bmatrix} = \vec{\psi}_{BCSZ}\,, \quad (15)$$

with

$$\vec{\psi}_{BCSZ} = \left[\psi_{0,BCSZ},\psi_{1,BCSZ},\psi_{2,BCSZ},\psi_{3,BCSZ}\right]^T\,. \quad (16)$$

Since $f(s,t) = 0$ along each solid line in Fig. 2, Eq. (14) can be manipulated to find a variable limit of integration with respect to t, $\hat{l}_t$, that is a function of s:

$$\hat{l}_t = -\frac{f_c + f_s s}{f_t + f_{st} s}\,. \quad (17)$$

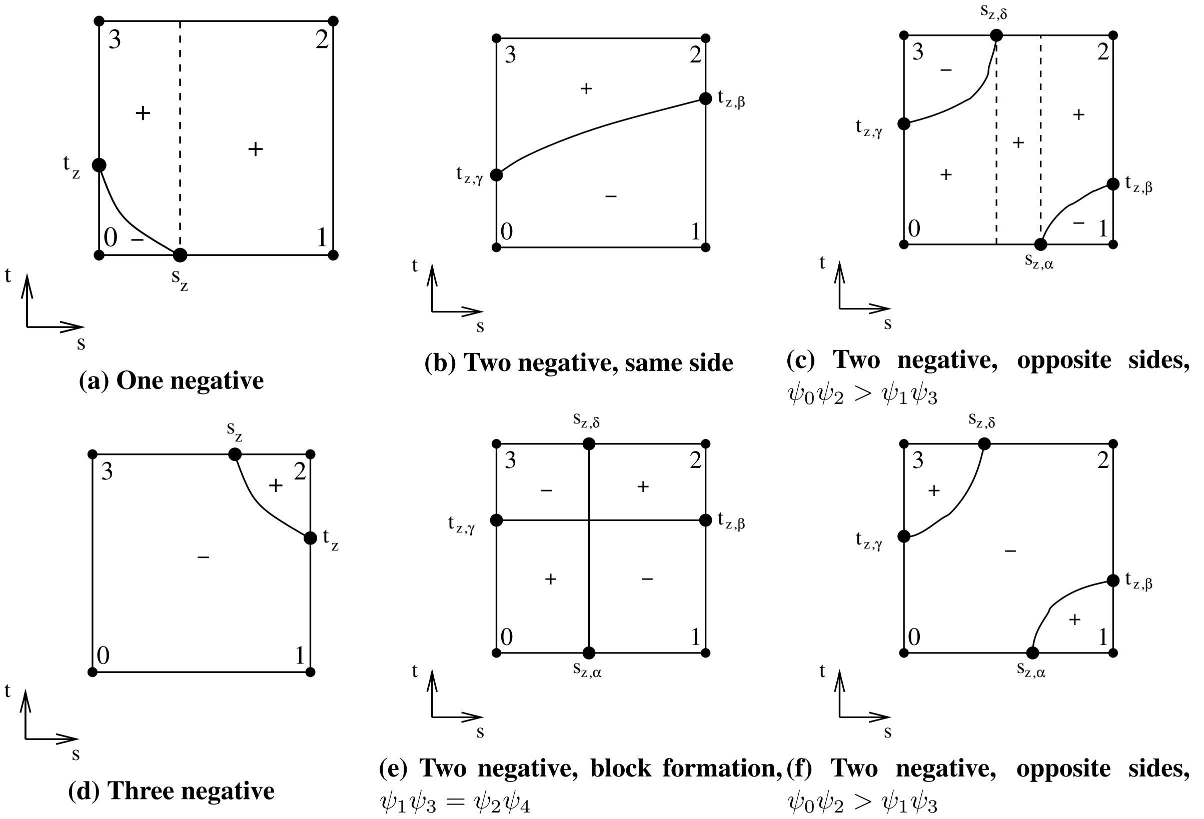

(a) One negative

(b) Two negative, same side

(c) Two negative, opposite sides, $\psi_0\psi_2 > \psi_1\psi_3$

(d) Three negative

(e) Two negative, block formation, $\psi_1\psi_3 = \psi_2\psi_4$

(f) Two negative, opposite sides, $\psi_0\psi_2 > \psi_1\psi_3$

Figure 2. BCSZ cell integration cases requiring special treatment.

Rather than evaluate each $\psi_{i,\mu}$, $\psi_{i,\eta}$, and $\psi_{i,M}$ integral, we seek a single, generic integrand that is only a function of s and t. We find this generic integrand by first expanding the specific $\widetilde{\psi}_{BCSZ}$integrand definitions of $\psi_{i,\mu}$, $\psi_{i,\eta}$, and $\psi_{i,M}$ over R. Starting with the integrand of $\psi_{i,\mu}$,

$$\widehat{\psi}_{BCSZ}(s,t)\left(\frac{\partial y}{\partial t}\frac{\partial B_i}{\partial s} - \frac{\partial y}{\partial s}\frac{\partial B_i}{\partial t}\right) = \left[f_c + sf_s + tf_t + stf_{st}\right]\ldots$$
$$\left(\left[y_{t,c} + sy_{t,s}\right]\left[b_{i,s,c} + tb_{i,s,t}\right] - \left[y_{s,c} + ty_{s,t}\right]\left[b_{i,t,c} + sb_{i,t,s}\right]\right)\ , \quad \text{(18a)}$$

then the $\psi_{i,\eta}$ integrand:

$$\widehat{\psi}_{BCSZ}(s,t)\left(\frac{\partial x}{\partial s}\frac{\partial B_i}{\partial t} - \frac{\partial x}{\partial t}\frac{\partial B_i}{\partial s}\right) = \left[f_c + sf_s + tf_t + stf_{st}\right]\ldots$$
$$\left(\left[x_{s,c} + tx_{s,t}\right]\left[b_{i,t,c} + sb_{i,t,s}\right] - \left[x_{t,c} + sx_{t,s}\right]\left[b_{i,s,c} + tb_{i,s,t}\right]\right)\ , \quad \text{(18b)}$$

and finally the $\psi_{i,M}$ integrand:

$$B_i(s,t)\widehat{\psi}_{BCSZ}(s,t)\left|J(s,t)\right| = \left[b_{i,c} + sb_{i,s} + tb_{i,t} + stb_{i,st}\right]\left[f_c + sf_s + tf_t + stf_{st}\right]\left[g_c + sg_s + tg_t\right]\ . \quad \text{(18c)}$$

In Eqs. (18) we have defined the following:

$$B_i(s,t) \quad = \quad b_{i,c} + sb_{i,s} + tb_{i,t} + stb_{i,st} \qquad \text{(19a)}$$

$$\begin{aligned}
\frac{\partial B_i}{\partial s} &= b_{i,s,c} + t b_{i,s,t} && \text{(19b)}\\
\frac{\partial B_i}{\partial t} &= b_{i,t,c} + s b_{i,t,s} && \text{(19c)}\\
|\mathbf{J}(s,t)| &= g_c + s g_s + t g_t && \text{(19d)}\\
\frac{\partial x}{\partial s} &= x_{s,c} + t x_{s,t} && \text{(19e)}\\
\frac{\partial x}{\partial t} &= x_{t,c} + s x_{t,s} && \text{(19f)}\\
\frac{\partial y}{\partial s} &= y_{s,c} + t y_{s,t} && \text{(19g)}\\
\frac{\partial y}{\partial t} &= y_{t,c} + s y_{t,s}\,. && \text{(19h)}
\end{aligned}$$

Using MATLAB [6], each integrand in Eqs. (18) is further expanded, then terms of equal degree bivariate polynomials, $s^m t^n$, with $0 \le m \le 3$, $0 \le n \le 3$, are collected. This allows us to calculate the twelve separate integrations of $\psi_{i,\mu}$, $\psi_{i,\eta}$, and $\psi_{i,M}$, as the multiplication of twelve unique sets of constants, $\mathbf{C}_{i,\mu}$, $\mathbf{C}_{i,\eta}$, and $\mathbf{C}_{i,M}$, multiplied by the integrations of a single set of bivariate polynomials, over R.

3.1.1 Symbolic integration versus numerical integration

Initially, MATLAB [6] symbolic algebra generated expressions for the integrations of the generic bivariate polynomials over R were used to evaluate $\psi_{i,\mu}$, $\psi_{i,\eta}$, and $\psi_{i,M}$. This worked well at low cell counts, but caused the $\widetilde{\psi}_{BCSZ}$non-linear iteration to fail at higher cell counts. To verify the MATLAB generated expressions, we compared the "exact" symbolic algebra generated results for calculating $\psi_{i,M}$ for $\vec{\psi}_{BCSZ} = [-2\ 0.1\ 200\ 10]^T$ to the value obtained using N_s Gauss quadrature points in s along the curved boundary. A two-point Gauss quadrature in t was used for each corresponding Gauss point in s (tensor product quadrature). An example of the quadrature layout is given in Fig. 3 for $N_s = 4$. In Fig. 4a, we plot $E_{i,quad}$, where:

$$E_i = \frac{|\psi_{i,sym} - \psi_{i,num}|}{|\psi_{i,sym}|}\,, \tag{20}$$

$\psi_{i,sym}$ is the evaluation of $\psi_{i,M}$ using the symbolic algebra generated expressions, and $\psi_{i,num}$ is the quadrature evaluation of $\psi_{i,M}$ using $2N_s + 4$ quadrature points. Compare the result of Fig. 4a to Fig. 4b, which plots $\widehat{E}_i$:

$$\widehat{E}_i = \frac{|\psi_{i,MAX} - \psi_{i,num}|}{|\psi_{i,MAX}|}\,, \tag{21}$$

where $\psi_{i,MAX}$ is the quadrature approximation of $\psi_{i,M}$ using Gauss quadrature and $N_S = 40$. It is clear that the "exact" symbolic evaluated expressions suffer from numerical round-off caused by taking the small difference of large numbers. As such, we prefer quadrature integration to evaluate cell integral quantities for the BCSZ scheme. However, for a fixed number of Gauss points in s, we cannot apriori estimate the error in our quadrature approximation of bivariate polynomial integrals over the region with a curved boundary. Gauss-Kronrod quadrature [7] allows for an estimate of the

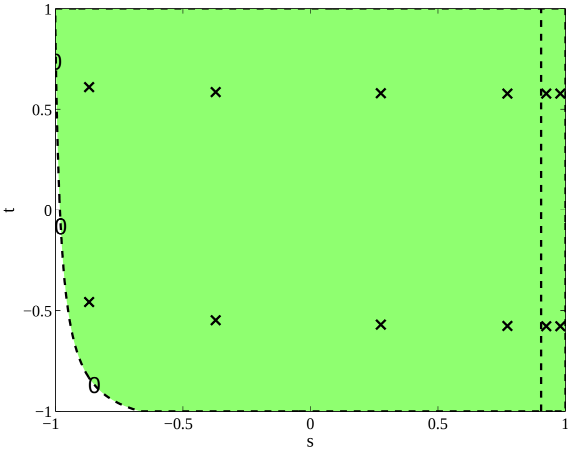

Figure 3. Quadrature point locations for $N_s = 4$ for quadrature integration test.

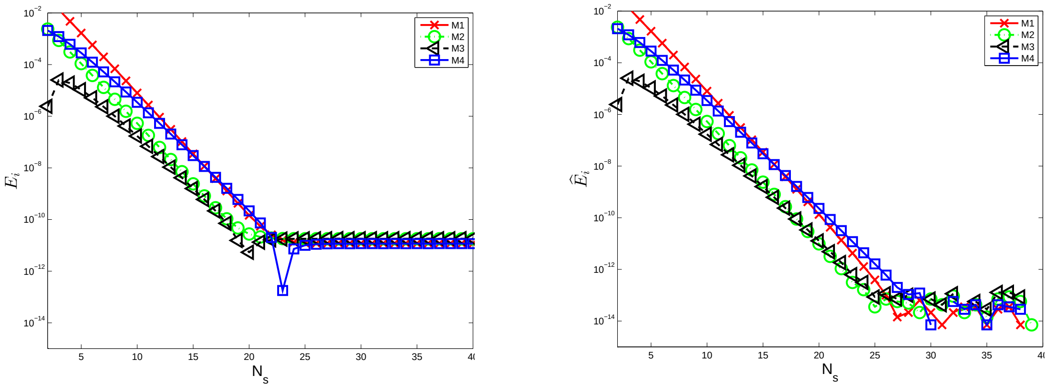

(a) E_i **for quadrature test.**

(b) $\widehat{E}_i$ **for quadrature test.**

Figure 4. Comparison of quadrature vs. exact integration errors.

quadrature error to the approximation of an integration. In practice, we now use the 7-point Gauss / 15-point Kronrod quadrature set in is s with a 2-point Gauss quadrature in t to integrate all BCSZ quantities. Along with sub-interval refinement, this integration strategy, and the decompositions shown in Fig. 2 allow for the computation of all BCSZ cell integral quantities to a tolerance less than our non-linear iteration tolerance.

3.2 BCSZ Edge Integration

Along any edge, there are four possible cases. Assuming that we are looking at edge α, but with easy translation to any other edge:

1. $\widehat{\psi}_{BCSZ} > 0$ along whole edge,

2. $\widehat{\psi}_{BCSZ} < 0$ along whole edge,

3. $\psi_{0,BCSZ} < 0$, $\psi_{1,BCSZ} > 0$, and

4. $\psi_{0,BCSZ} > 0$, $\psi_{1,BCSZ} < 0$.

Case one is straightforward and identical to the integration used by the UBLD scheme. Case two is by definition, zero along the integral. Cases three and four are handled by first determining s_z, such that $\widehat{\psi}_{BCSZ}(s_z, -1) = 0$:

$$s_z = \frac{\psi_{0,BCSZ} + \psi_{1,BCSZ}}{\psi_{0,BCSZ} - \psi_{1,BCSZ}} \tag{22}$$

Then a two point Gauss quadrature is mapped to the interval $[s_z, 1]$ for case 3 and $[-1, s_z]$ for case 4, and the integral of $\psi_{i,\alpha}$ is approximated (exactly) using function evaluations at the mapped quadrature points.

4 NUMERICAL RESULTS

We now present computational results for a simple test problem, a $10\ [cm] \times 10\ [cm]$ void, S_4 level symmetric angular quadrature, with vacuum boundary condition on the left, top, and right sides, incident angular flux of $1\ [n/(cm^2 - sec - ster)]$ in the direction of $\mu = 0.868890300722$, $\eta = 0.350021174582$ along the bottom edge, vacuum conditions along the bottom edge for all other directions along the bottom face. In Fig. 5 we compare the results of the UBLD, FLBLD, and BCSZ schemes on an orthogonal mesh of 64×64 cells, plotting the cell average scalar fluxes on a logarithmic scale. The negativities and oscillations of the UBLD scheme are obvious. The BCSZ and FLBLD solutions are both strictly non-negative. However, the FLBLD scheme has a significant amount of numerical diffusion, whereas the BCSZ scheme maintains a sharp boundary at the discontinuity.

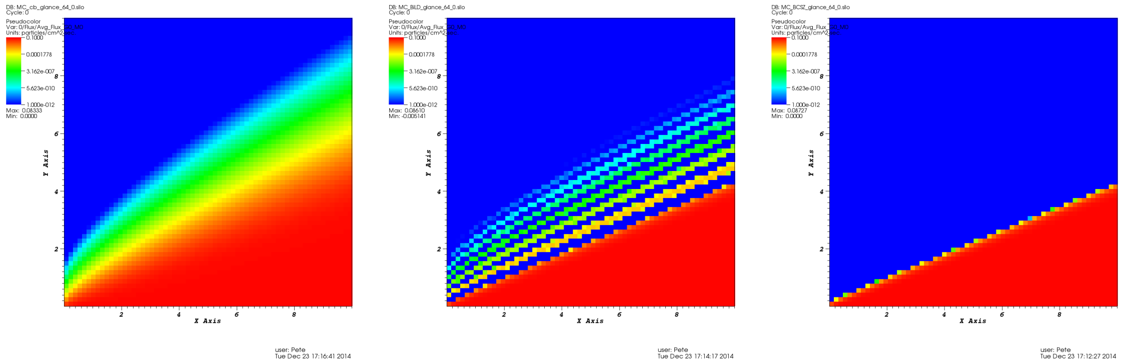

(a) FLBLD solution **(b) UBLD solution** **(c) BCSZ solution**

Figure 5. 64×64 **mesh cell cell average scalar flux solutions**

In Fig. 6 we show the BCSZ and UBLD cell average scalar flux solutions on a 25 cell × 25 cell mesh with each interior vertex perturbed to create an unstructured mesh. Figure 6 shows the BCSZ scheme is capable of being used for unstructured mesh problems. Though the BCSZ solution exhibits some numerical diffusion in Fig. 6, it is a result of the mesh, as the UBLD scheme exhibits the same increase in numerical diffusion, while also demonstrating the negativities and oscillations of the UBLD solution.

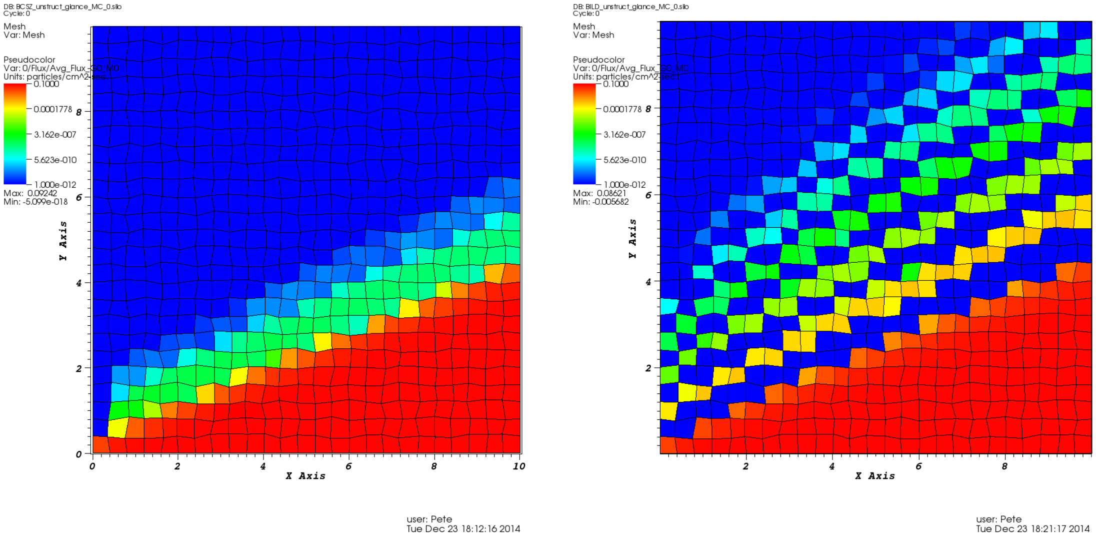

(a) BCSZ solution on unstructured grid.

(b) UBLD solution on unstructured grid.

Figure 6. Glancing void solutions with 25×25 mesh cells.

Finally, in Fig. 7, we plot an E_{ϕ_A},

$$E_{\phi_A} = \sqrt{\sum_{c=1}^{N_c ells} \Delta x_c \Delta y_c (\widetilde{\phi}_A - \phi_{A,exact})^2} \tag{23}$$

an L_2 like norm of the average scalar flux in each cell for the UBLD, FLBLD, and BCSZ schemes on orthogonal meshes. In Eq. (23), $\widetilde{\phi}_A$ is the computed cell average scalar flux for a particular scheme in cell c, Δx and Δy are the respective cell widths of cell c, and $\phi_{A,exact}$ is the analytic cell average scalar flux in cell c. From Fig. 7, we determine that BCSZ is more accurate than UBLD, while both UBLD and BCSZ are significantly more accurate than FLBD. Also, we verify that all methods reach the same asymptotic order of convergence, $h^{1/4}$. All of the methods considered converge the error in the cell average angular flux at this low rate due to the discontinuity in the analytic solution.

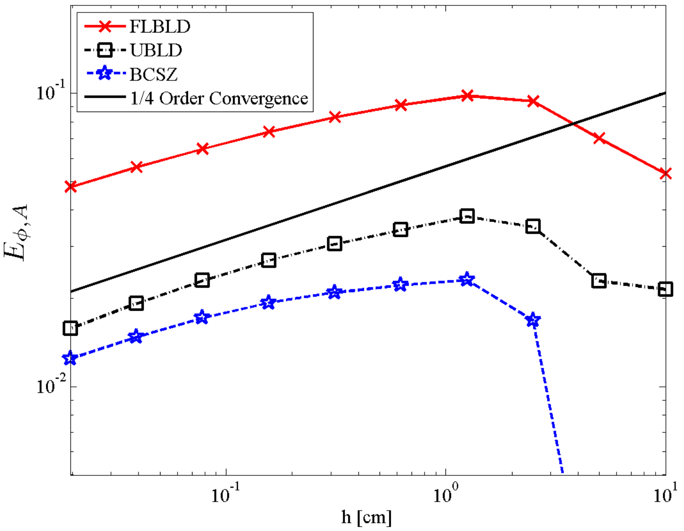

Figure 7. Convergence of cell average scalar flux on orthogonal grids.

5 CONCLUSIONS

The BCSZ scheme produces strictly non-negative solutions that are at least as accurate as UBLD solutions. To date, the accuracy of the BCSZ scheme has only been measured against pure absorber/void test problems. We are currently awaiting the completion of a modified interior penalty diffusion synthetic acceleration (MIP DSA) implementation [8] in the TAMU developed S_N solver, PDT [9], to apply the BCSZ to more interesting neutron transport and radiative transfer problems. We see numerous opportunities for future research going forward including:

1. comparing the efficiency of our current/near term solution methodology (fixed point iteration with MIP DSA) to the solution methodology proposed by Bruss, et. al [10] and
2. generalizing BCSZ to higher order, Q_N trial spaces through the extension of our adaptive quadrature integration scheme,

6 ACKNOWLEDGMENTS

Portions of this work were funded by the Department of Energy CSGF program, adminstered by the Krell Institute, under grant DE-FG02-97ER25308.

7 REFERENCES

[1] M. L. Adams, “Discontinuous Finite Element Transport Solutions in Thick Diffusive Problems,” *Nuclear Science and Engineering*, **137**, pp. 298–333 (2001).

[2] E. D. Fichtl, J. S. Warsa, and J. D. Densmore, "The Newton-Krylov Method Applied to Negative-Flux Fixup in S_N Transport Calculations," *Nuclear Science and Engineering*, **165**, pp. 331–341 (2010).

[3] P. G. Maginot, J. E. Morel, and J. C. Ragusa, "A Non-negative Moment Preserving Spatial Discretization Scheme for the Lienarized Boltzmann Transport Equation in 1-D and 2-D Cartesian Geometries," *Journal of Computational Physics*, **231**, pp. 6801–6826 (2012).

[4] T. A. Wareing, E. W. Larsen, and M. L. Adams, "Diffusion Accelerated Discontinuous Finite Element Schemes for the S_N Equations in Slab and X,Y Geometries," *Proc. International Topical Mtg. on Advances in Mathematics, Computations and Reactor Physics*, Pittsburgh, PA, April 28-May 2, 1991.

[5] M. L. Adams, "Subcell Balance Methods for Radiative Transfer of Arbitrary Grids," *Transport Theory and Statistical Physics*, **26**, pp. 385–431 (1997).

[6] Mathworks, "MATLAB R-2011a," 2011.

[7] T. N. L. Patterson, "The Optimum Addition of Points to Quadrature Formulae," *Mathematics of Computation*, **22**, pp. 847–856 (1968).

[8] M. W. Hackemack and J. C. Ragusa, "A DFEM Formulation of the Diffusion Equation on Arbitrary Polyhedral Grids," *Proceeding of ANS 2014 Winter Meeting*, Anaheim, California, November 9-13, 2014.

[9] W. D. Hawkins, T. S. Bailey, and et al., "Validation of Full-Domain Massively Parallel Transport Sweep Algorithms," *Proceeding of ANS 2014 Winter Meeting*, Anaheim, California, November 9-13, 2014.

[10] D. E. Bruss, J. E. Morel, and J. C. Ragusa, "S_2SA Preconditioning for the S_N Equations with Strictly Non-negative Spatial Discretization," *Journal of Computational Physics*, **273**, pp. 706–719 (2014).